ACS NANO
Cite This: ACS Nano 2018, 12, 1920−1927
www.acsnano.org

ARTICLE

Optical Anapole Metamaterial

Pin Chieh Wu,[†] Chun Yen Liao,[‡] Vassili Savinov,[§] Tsung Lin Chung,[‡] Wei Ting Chen,[‡] Yao-Wei Huang,[†] Pei Ru Wu,[‡] Yi-Hao Chen,[‡] Ai-Qun Liu,[∥] Nikolay I. Zheludev,[§,⊥] and Din Ping Tsai*[,†,‡,#]

[†]Research Center for Applied Sciences, Academia Sinica, Taipei 11529, Taiwan
[‡]Department of Physics, National Taiwan University, Taipei 10617, Taiwan
[§]Optoelectronics Research Centre and Centre for Photonic Metamaterials, University of Southampton, Southampton SO17 1BJ, U.K.
[∥]School of Electrical and Electronic Engineering, Nanyang Technological University, Singapore 639798, Singapore
[⊥]TPI and Centre for Disruptive Photonic Technologies, Nanyang Technological University, Singapore 637371, Singapore
[#]College of Engineering, Chang Gung University, Taoyuan 33302, Taiwan

Supporting Information

ABSTRACT: **The toroidal dipole is a localized electromagnetic excitation independent from the familiar magnetic and electric dipoles. It corresponds to currents flowing along minor loops of a torus. Interference of radiating induced toroidal and electric dipoles leads to anapole, a nonradiating charge-current configuration. Interactions of induced toroidal dipoles with electromagnetic waves have recently been observed in artificial media at microwave, terahertz, and optical frequencies. Here, we demonstrate a quasi-planar plasmonic metamaterial, a combination of dumbbell aperture and vertical split-ring resonator, that exhibits transverse toroidal moment and resonant anapole behavior in the optical part of the spectrum upon excitation with a normally incident electromagnetic wave. Our results prove experimentally that toroidal modes and anapole modes can provide distinct and physically significant contributions to the absorption and dispersion of slabs of matter in the optical part of the spectrum in conventional transmission and reflection experiments.**

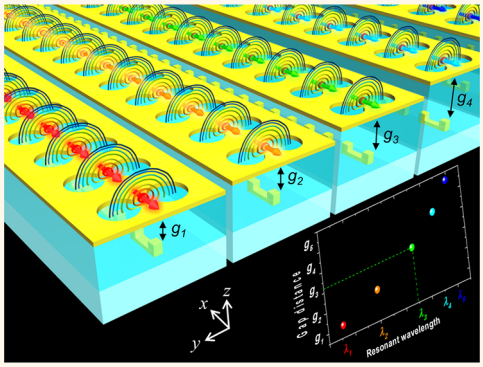

KEYWORDS: *toroidal dipole, anapole mode, plasmonic metamaterial, magnetic dipole, split-ring resonator*

Static toroidal dipole was first proposed in 1957 in the context of nuclear physics.[1−3] Dynamic (induced) toroidal dipole is an independent term in the family of electrodynamic multipole expansion.[4] It is associated with a nonvanishing longitudinal term $\vec{r}\cdot\vec{j} \neq 0$, where $\vec{r}$ and $\vec{j}$ are the position vector and the current density induced by the external stimuli, respectively. Hence, the toroidal dipole is naturally different from the electric and magnetic multipoles that are associated with nonvanishing induced charge density, $\rho \neq 0$, and nonzero induced transverse current density, $\vec{r}\times\vec{j} \neq 0$, respectively (see box 2 in ref 4). Historically, the toroidal dipolar response was neglected as a contributor to the electromagnetic response of matter because the corresponding toroidal transition matrix elements tend to be weak for atoms and small molecules. It has been proven that the near-field characteristics and electromagnetic multipoles can be artificially tailored through plasmonic meta-structures.[5−8] A few years ago, the toroidal dipole excitation was, for the first time, experimentally observed as the dominant term in the electromagnetic response of purposely designed metamaterials[9−11] in the microwave region.[12] Subsequently, the toroidal resonances have also been pushed to terahertz and optical frequencies with metallic and dielectric metamaterials.[13−17] The destructive interference between colocated and coaligned toroidal and electric dipoles yield a nonradiating anapole mode,[18−20] which was also first discovered in microwave range.[21] So far, most of the published results explored structures where the toroidal dipoles are generated perpendicular to the surface of the metamaterials.[16,22−24] Such excitations are difficult to couple to external radiation without resorting to complex excitation geometries. Here, we demonstrate a quasi-planar plasmonic metamaterial exhibiting induced transverse toroidal response and associated resonant anapole response in the optical part of the spectrum, driven by normal incident light.

The toroidal metamaterial reported here is a multilayered structure containing a planar array of vertical split-ring resonators (VSRRs) suspended in a dielectric medium and covered with a perforated gold film. The perforations (apertures) in the gold film are dumbbell-shaped and are aligned to VSRRs (see Figure 1a). At resonance, the normal incident plane-wave radiation, polarized

Received: December 14, 2017
Accepted: January 26, 2018
Published: January 27, 2018

DOI: 10.1021/acsnano.7b08828
ACS Nano 2018, 12, 1920−1927

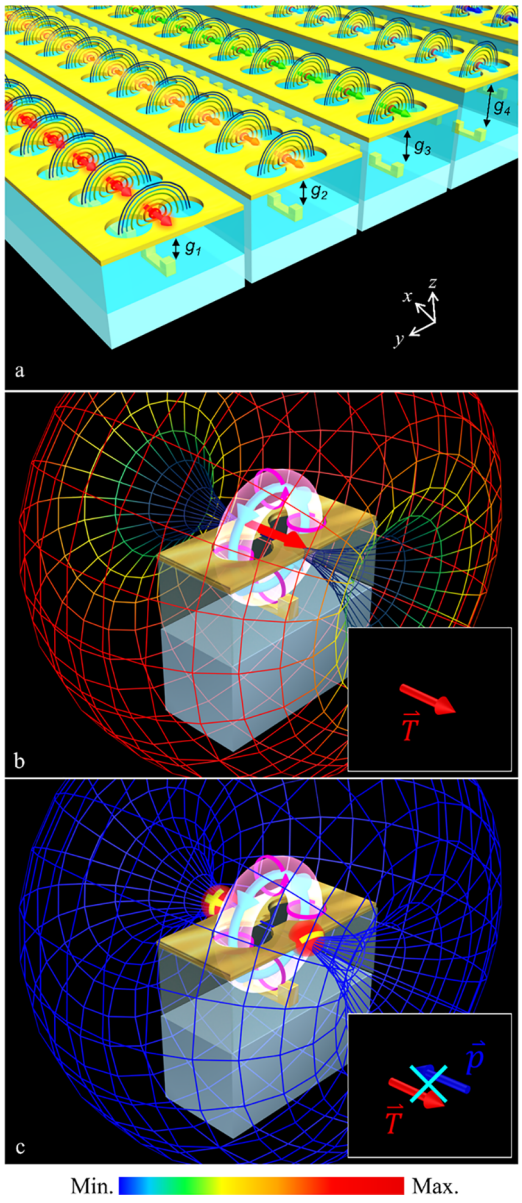

Figure 1. (a) Schematic for the toroidal metamaterial, which consists of a gold film perforated by dumbbell-shaped apertures, situated above a planar array of VSRRs suspended in a dielectric spacer layer. At resonance, the metamaterial supports the toroidal dipole excitations. The color arrows and the streamlines show the orientation of induced toroidal dipoles and the corresponding magnetic field distribution, respectively. The response of the metamaterial can be tuned by changing the gap size *g*. (b) The radiation pattern of a point-like toroidal dipole is superimposed with a single metamaterial unit cell and a schematic depiction of the toroidal dipole excitation (pink torus and the blue circulating magnetic field). Inset shows the orientation of the toroidal dipole that corresponds to the radiation pattern in the main figure. (c) The nonradiating anapole mode, which is induced when the coaligned electric and toroidal dipoles radiate, is in antiphase (inset). The charges of the electric dipole are shown by red spheres. The color mesh in (b) and (c) represents radiation intensity. The radiation intensity in (c) is much weaker than that of (b) because of the destructive interference between electric and toroidal dipoles.

along the VSRRs, shall induce toroidal dipole excitations along the same direction, as illustrated in Figure 1a. Such excitations will be coupled to free-space radiation and will, therefore, directly contribute to the optical response of the metamaterial. Figure 1b shows the radiation pattern of a point-like toroidal dipole superimposed with the single unit cell of the metamaterial. The radiation pattern of the toroidal dipole is identical to that of the electric dipole. Combining these two dipoles, with appropriate amplitude and phase relationship, therefore allows a destructive interference, resulting in the so-called anapole mode with strong fields in the vicinity of the source and vanishingly small far-field emission, as shown in Figure 1c. The metamaterial presented here includes a tunable parameter, the spacing between VSRRs, and the perforated gold film (see Figure 1a), which allows the resonant wavelength of both the toroidal dipole and the nonradiating anapole mode to be tuned. This parameter can be adjusted by controlling the thickness of the deposited dielectric spacer. This demonstration offers flexibility and reliability in the optimization of the sample geometry of the anapole-supporting plasmonic nanostructures.

RESULTS AND DISCUSSION

To motivate the design of the metamaterial depicted in Figure 1, we first consider the modeled response of a simpler sample that consists of only the dumbbell-perforated gold film on the dielectric substrate, as shown in Figure 2a. The metamaterial is driven by horizontally polarized (*x*-polarized in Figure 2a) plane-wave radiation at normal incidence. The incident light induces charge oscillations at the two central edges of the apertures (green "+" and "−" in Figure 2a), leading to a strong horizontal electric dipole. The charge oscillations are accompanied by counter-rotating current oscillations along the rims of the two circular holes that make up the apertures (blue circulating arrows in Figure 2a), in turn, this leads to a pair of counter-oriented out-of-plane magnetic dipoles (red arrows in Figure 2a). A pair of counter-oriented magnetic dipoles, corresponding to a superposition of equal-magnitude magnetic quadrupole and toroidal dipole,[17] is shown in Figure 2b. Therefore, the response of the metamaterial is dominated by a combination of electric and toroidal dipoles as well as magnetic quadrupole. Figure 2c shows the calculated transmission and reflection spectra of dumbbell-aperture metamaterial (horizontal polarization), which we decomposed into contributions of individual multipoles.[25] Here, the origin position in the *xy*-plane is chosen based on the symmetry (at the center of the unit cell), while the origin position along the *z*-axis is assumed to be at the top of the metamaterial (just above the gold film). The main objective of the multipole decomposition is to represent a localized electromagnetic excitation in a way that is irreducible under 3-dimensional (3D) rotations. The source of electromagnetic excitation is the charge-current density, which is a 4-dimensional vector field that is subject to one constraint in the form of the charge conservation equation. In practice, this means that current density can be regarded as a completely arbitrary 3D vector field and the charge density is then obtained from it. To provide a full multipole decomposition of an arbitrary vector field, one needs three multipole families, that is, electric, magnetic, and toroidal dipoles.[26] In Figure 2d, the strength of multipole excitations is compared by considering power scattered over the full 4π solid angle.[12,26] As expected from mode analysis in Figure 2a,b, the main contributors to the metamaterial response are the electric dipole and a superposition of closely matched toroidal dipole and magnetic quadrupole. The validity of the multipole decomposition shown in Figure 2d is verified by adding all multipole fields to reproduce the metamaterial response (see Figure 2c).

The dumbbell-aperture alone, shown in Figure 2, cannot produce a dominant toroidal dipole response. However, combining

DOI: 10.1021/acsnano.7b08828
ACS Nano 2018, 12, 1920−1927

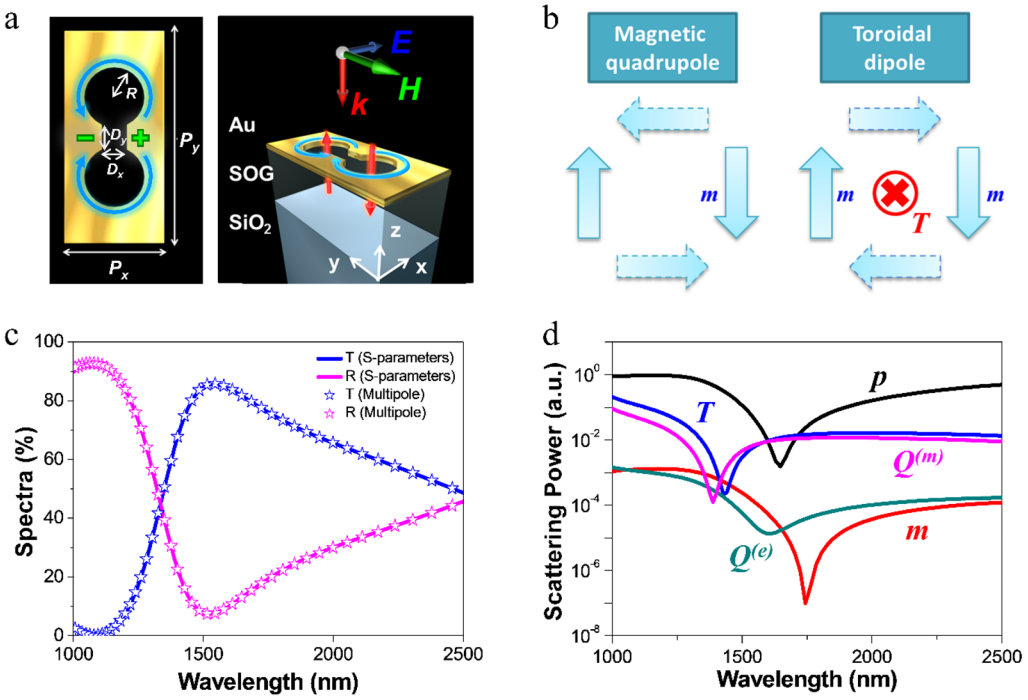

Figure 2. Electromagnetic responses of dumbbell-shaped apertures. (a) Left: The schematic for the dumbbell-shaped aperture. The feature sizes of metallic structures: P_x = 400 nm, P_y = 850 nm, R = 130 nm, D_x = 50 nm, D_y = 60 nm. Right: Orientation of incident field and the 30 nm-thick dumbbell-shaped aperture. (b) Representation of magnetic quadrupole and toroidal dipole in terms of magnetic dipoles. (c) Transmission and reflection spectra of metamaterial from direct calculation (solid lines) and from summing individual multipole contributions (stars). (d) Calculated scattered power for individual electromagnetic multipoles induced in metamaterial (unit cell) by the incident radiation. *p*: electric dipole, *m*: magnetic dipole, $Q^{(e)}$: electric quadrupole, $Q^{(m)}$: magnetic quadrupole, *T*: toroidal dipole.

the dumbbell-apertures with VSRR,[27,28] i.e., changing the metamaterial design from Figure 2a to Figure 1a, breaks the symmetry, resulting in an enhanced toroidal dipole and a suppressed magnetic quadrupole. Indeed, VSRRs generate a strong magnetic dipolar response under normal illumination when the incident electric field is parallel to the opening gap.[29−31] Combining the magnetic dipole, induced in VSRR, with the two magnetic dipoles, that are due to the counter-rotating currents in the dumbbell-aperture, results in the predominantly toroidal excitation of the merged structure (see inset in Figure 3a). The transmission and reflection spectra of the combined metamaterial (VSRR and dumbbell-apertures) are shown in Figure 3a,b as a function of radiation wavelength and separation between the VSRRs and the perforated gold film (gap size, see Figure 1a). Figure 3c,d shows the distribution of the magnetic field induced in the unit cell of the combined metamaterial at toroidal resonance, confirming the picture discussed above. Indeed, at resonance, the response of the dumbbell-aperture results in two counter-oriented out-of-plane magnetic dipoles, while the contribution of the VSRR corresponds to the *y*-polarized magnetic dipole. The net effect is a tight loop of the oscillating magnetic field (Figure 3d), a hallmark of the toroidal dipole response. An important feature of the metamaterial's resonant response here is that the mode (i.e., electromagnetic field), associated with a strong toroidal dipole response, extends beyond the physical boundaries of the metamaterial (Figure 3d). This is of great practical significance, since one can exploit this "leaking" field for applications, such as in sensing. By contrast, in dielectric toroidal/anapole metamaterials reported previously,[16,24,32−34] the field remains hidden within the bulk of the dielectric, greatly reducing the practical utility of these devices. It is worth mentioning that in the case of vertical polarization of the incident field (along *y*-axis in Figure 1a), electric quadrupole and magnetic dipole dominate the radiated fields (see Supporting Information).

Figure 4a shows the power scattered by individual multipoles that form the response of the planar toroidal metamaterial (see Figure 3). Toroidal dipole emission, which is about 85.1 and 2.5 times, respectively, stronger than that of electric and magnetic dipoles, clearly dominates in the window around 1350 nm (olive region in Figure 4a). Next, we consider interference between electric and toroidal dipoles. The scattered powers of these two multipoles are equal at around 1400 nm (dashed line in Figure 4a), while all other multipole contributions are relatively small. The phase difference between emissions of toroidal and electric dipoles, presented in Figure 4a (bottom graph), shows that at that wavelength, the two dipoles interfere destructively, resulting in a single resonant dip in the scattering power spectrum (bottom panel in Figure 4a). This is the so-called anapole mode, which is manifested as simultaneous enhancement of the near-field and suppression of the far-field. The suppression of the far-field scattering is also verified by calculating the far-field scattering cross-section (and extinction spectra, see Supporting Information) from a single unit structure, as shown in Figure 4b. The spectral position of the anapole mode of the planar toroidal metamaterial depends on the separation between VSRRs and the perforated gold film (gap size; see Figure 1a), as shown in Figure 4c.

The relationship between gap size and strength of the toroidal dipole response in planar toroidal metamaterial is further investigated in Figure 5. Figure 5a shows the extent to which toroidal dipole scattering can dominate over other multipoles as a function of gap size, revealing that dominant toroidal dipole response is only possible when VSRR is close to the perforated gold film. At close proximity, the effect of VSRR is to contribute to creating the tight oscillating loop of the magnetic field (Figure 3d), which leads to

DOI: 10.1021/acsnano.7b08828
ACS Nano 2018, 12, 1920−1927

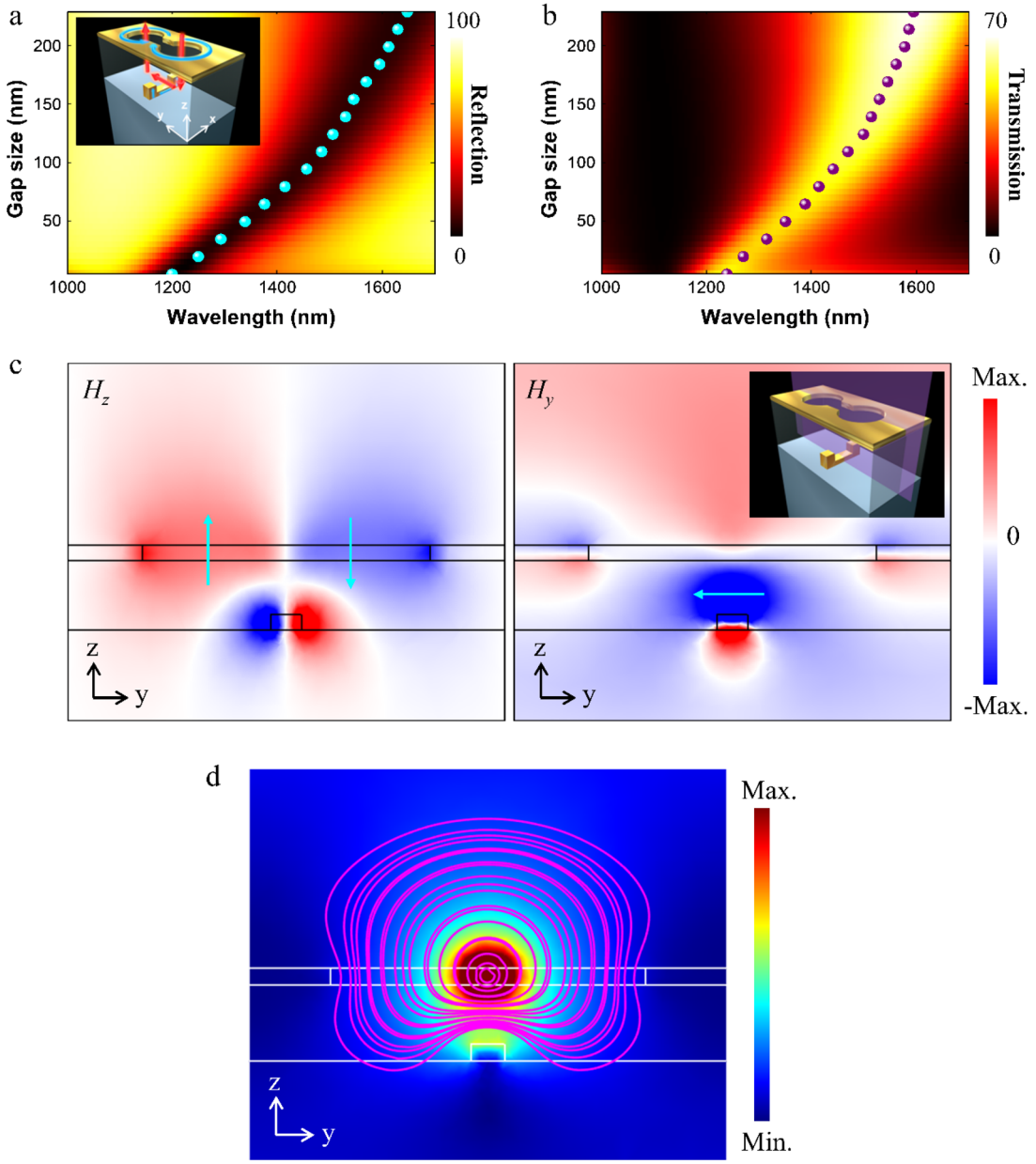

Figure 3. Electromagnetic response of planar toroidal metamaterial. (a) Reflection and (b) transmission spectra for toroidal metamaterials as a function of gap size (defined in Figure 1a). Cyan and purple dots indicate the reflection dip and transmission peak computed by first decomposing the metamaterial response into contributions of individual multipoles, and then adding the multipole fields together to recover the net response. Inset: Schematic for the toroidal metamaterial. The red arrows and the cyan circulating arrows indicate the induced magnetic dipoles and surface currents, respectively. The distribution of induced magnetic field and electromagnetic energy density in the vicinity of metamaterial unit cell, at toroidal dipole resonance, are shown in (c) and (d), respectively. The gap size for the structure is 50 nm. Purple lines indicate the configuration of the magnetic field. Cyan arrows present the direction of induced magnetic dipoles. Inset in (c): Schematic for the observation plane (marked as a semitransparent purple plane) of (c) and (d).

toroidal dipole excitation. When the gap size is increased the oscillations of VSRR start to fall behind those of the dumbbell-aperture (a phase difference appears), which favors the magnetic quadrupole. Hence, at a gap size of 20 nm, the toroidal dipole emerges as the dominant multipole at wavelengths around 1270 nm, whereas at a gap size of 635 nm, it is the magnetic quadrupole that dominates at around 1900 nm (see Figure 5b and the Supporting Information Movie).

Finally, we experimentally examine the optical properties of the proposed planar toroidal metamaterials. Figure 6a shows the top view SEM image of the fabricated sample. The integrity and accuracy of the multilayer toroidal metamaterials is confirmed by cutting a cross-section in the fabricated sample using focused ion beam (FIB) milling. Figure 6b displays an oblique SEM image of metamaterial cross-section, with 52° tilt, showing an accurate alignment between different steps of the e-beam lithography process. The measured spectra for the toroidal metamaterials with a 50 nm gap size (as defined in Figure 1a) are shown in Figure 6c. Metamaterial resonance occurs at 1389 nm, which is in good agreement with modeling results shown in Figure 3a. The slight shift and broader resonance in the experimental measurements arise as a result of inevitable variations in metamaterial dimensions and roughness of the fabricated sample. The dependence of material losses on the anapole mode excitation is

DOI: 10.1021/acsnano.7b08828
ACS Nano 2018, 12, 1920−1927

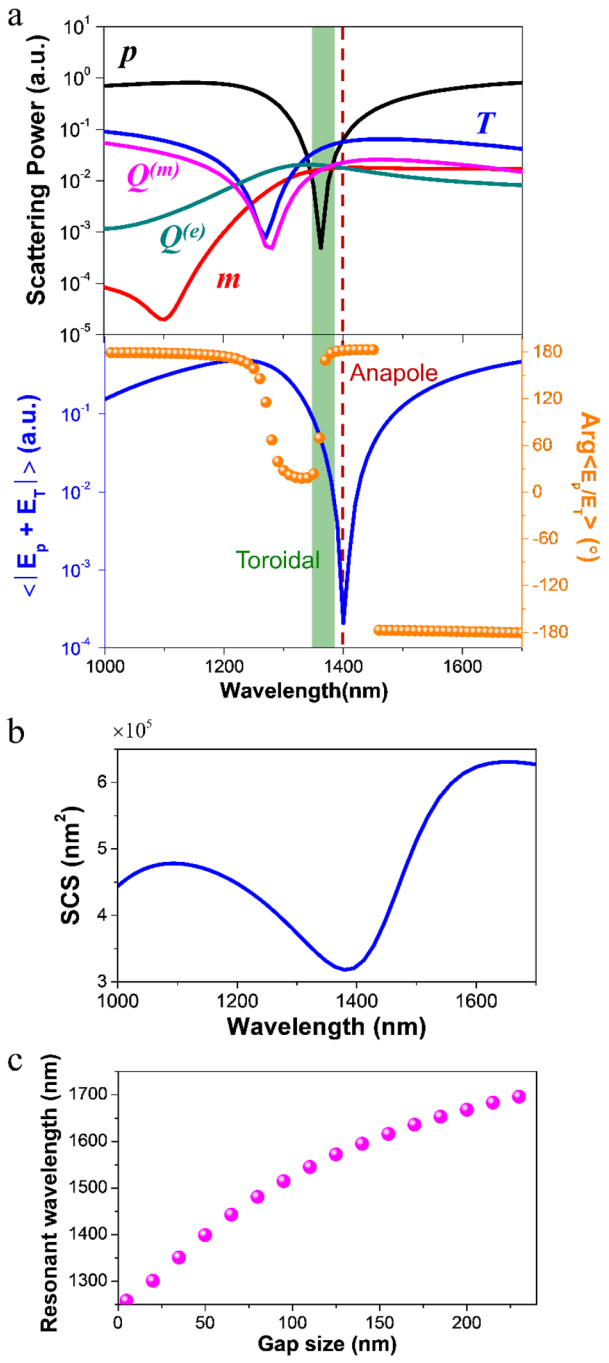

Figure 4. Multipole response of plasmonic toroidal metamaterial. (a) (Top) Scattering power of electromagnetic multipoles when gap size is 50 nm, and (bottom) the average scattering power (blue curve) and phase difference (orange dots) from the electric fields radiated from electric and toroidal dipoles. The olive area and dark-red dashed line denote the resonance region and wavelength of the toroidal dipole and anapole mode, respectively. (b) Far-field scattering cross-section. It is defined as the ratio between powers of the radiation scattered by a single unit cell of metamaterial and incident radiation. (c) The spectral position of the anapole mode as a function of gap size (defined in Figure 1a).

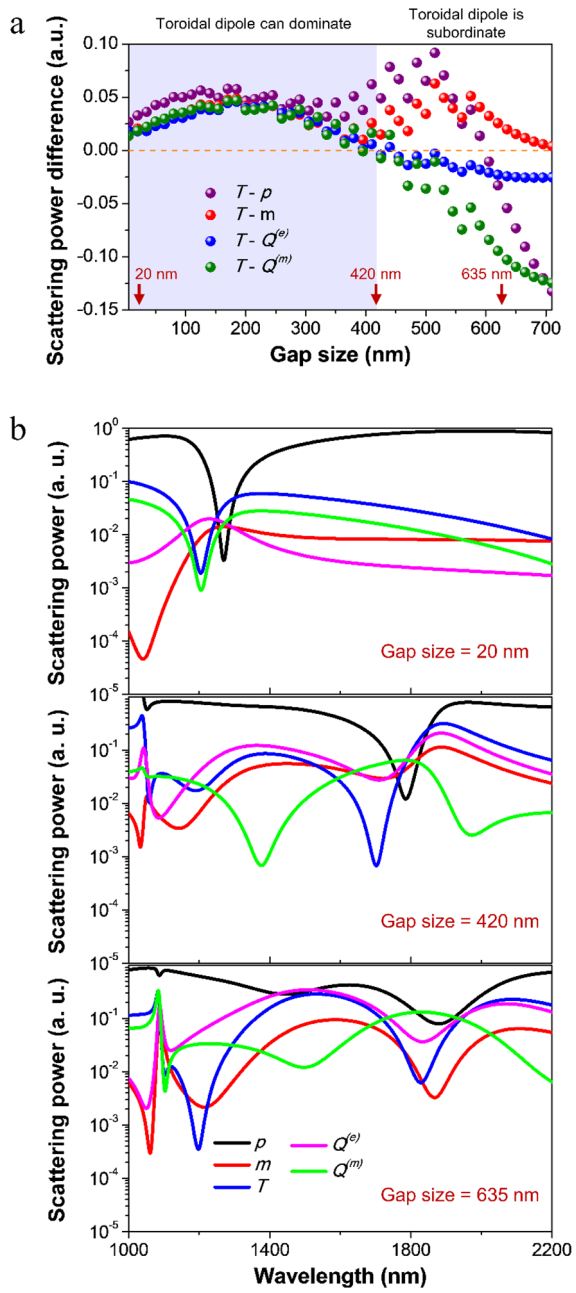

Figure 5. Electromagnetic multipole evolution with different gap sizes. (a) Scattering power difference between toroidal dipole and other electromagnetic multipoles at the dip position of the electric dipole. The area with purple background indicates the region where toroidal dipolar response can dominate the spectrum (at a certain resonant wavelength). (b) Calculated scattering power for the five leading electromagnetic multipoles when the gap size is 20 (top panel), 420 (middle panel), and 635 (bottom panel).

investigated in the Supporting Information. On the other hand, one can clearly observe a minimum far-field scattering intensity (defined as the reflection plus transmission) at the wavelength of the anapole mode in the experimental spectra, which agrees with the numerical prediction shown in Figure 4b.

The precision-engineered electromagnetic nanostructure presented here enables the excitation of the toroidal dipole and the anapole modes at the wavelength of choice. The suppression of radiation losses offered by the multipole interference in the anapole modes could find many applications. For example, the high energy confinement at the wavelength of the nonradiating anapole mode enables significantly enhancing the nonlinear response.[35,36] The great field confinement, which leads to a strong gradient force around the plasmonic structures, could be applied in optical trapping.[37] The optical response with high

DOI: 10.1021/acsnano.7b08828
ACS Nano 2018, 12, 1920−1927

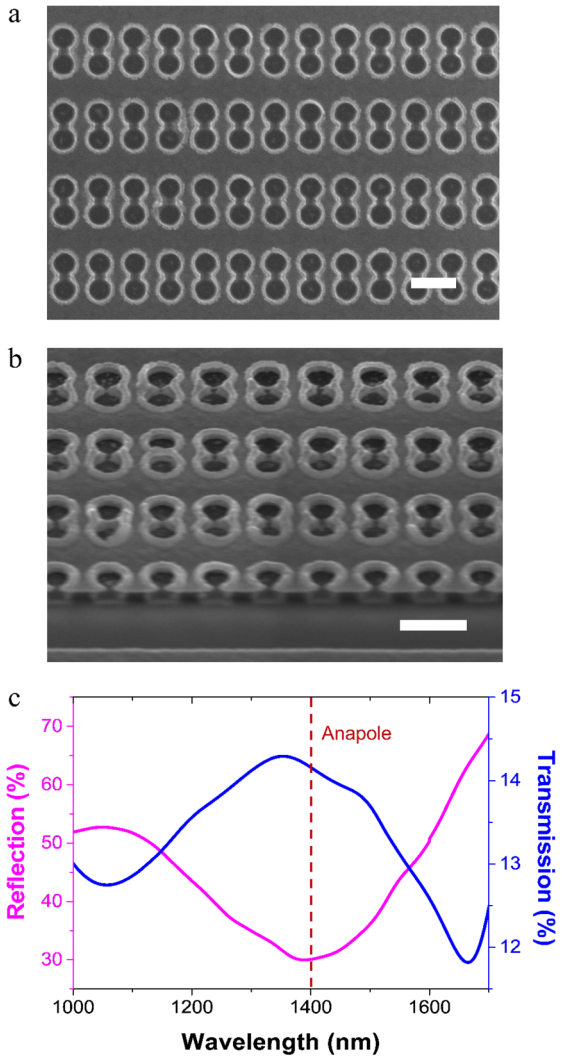

Figure 6. (a) Top and (b) tilted views of SEM images of a fabricated sample with a 50 nm gap size. Scale bars: 500 nm. (c) Measured far-field spectra of the plasmonic toroidal metamaterials under *x*-polarized illumination (compare to Figure 1a). The dark-red dashed line represents the resonant wavelength of the anapole mode from the numerical predication.

quality-factor can further benefit the development of nanophotonic light sources, including lasing spasers, etc.[38,39] In our design, with the plasmonic mode being accessible in free space (close to the sample), it is also applicable to sensing applications, such as surface enhanced Raman scattering (SERS). Development of toroidal spectroscopy, which is highly desirable to observe and analyze the toroidal resonances in natural matters, is also feasible due to the efficient couple between anapole metamaterials and interested toroidal molecules. Furthermore, localized toroidal excitations, such as those demonstrated here, are a natural starting point for experimental study of the exotic topological configurations known as electromagnetic focused doughnut pulses.[4]

CONCLUSIONS

In summary, we have designed, analyzed, and fabricated the planar plasmonic metamaterial, which supports transverse toroidal dipole and anapole excitations that dominate the metamaterial's resonant response in the optical part of the spectrum. All significant properties of the anapole metamaterial can be tuned through a single well-defined geometrical parameter, which can be controlled to a great precision during fabrication. It benefits the design of the optical metamaterials with the desired multipole response, while the others are suppressed on purpose. Our technology offers fine control over the radiation loss, and near-field enhancement in nanophotonics. This work could therefore have immediate applications in sensing, nonlinear optics, and optomechanics.

METHODS

Sample Fabrication. A ZEP 520A layer was spin coated at 4000 rpm onto a fused silica substrate and then was baked on a hot plate for 5 min at 180 °C. Subsequently, an Espacer layer was spin coated at 1500 rpm onto the ZEP520A layer. Espacer is an organic polymer with high conductivity to reduce the positional error during the e-beam exposure process. An e-beam writing system at the acceleration voltage of 100 keV with 30 pico-ampere of current was used. The base rod of VSRR was defined by the first e-beam exposure and lift-off process. The two prongs of VSRR were fabricated by the second e-beam exposure and lift-off process. In our case, we used spin on glass (SOG) for the spacer layer to isolate the VSRR and dumbbell-shaped structure. SOG layer was subsequently spin-coated at 3000 rpm onto a fused silica substrate with a fabricated VSRR array, and then it was baked on a hot plate for 3 min at 200 °C. The reactive ion etching (SAMCO RIE-10N, reaction gas was CF_4, flow rate was 50 sccm, pressure was 0.78 kpa, RF power was 70 W, and etching time was 1 min) was used to attain the appropriate thickness (50 nm) of SOG layer we needed. Then, we used RF sputter to deposit 30 nm gold films onto the sample, and spin coated ZEP520A over the gold film. We used the third e-beam exposure to process the dumbbell-shaped holes in the same area, which were fabricated after RIE etching (ANELVA DEM-451T, reaction gas: Ar, flow rate: 20 sccm, pressure: 0.02 mbar, RF power: 100 W, and etching time: 3 min). Here, the photoresist (ZEP520A) was used as the antietch layer.

Measurement. The measurement data were carried out by Bruker VERTEX 70 Fourier-transform infrared spectrometer equipped with Bruker HYPERION 2000 infrared microscope (15 × Cassegrain objective, numerical aperture NA = 0.4, near-infrared polarizer, and an InGaAs and MCT detector). An iris was used to collect the incident light to a square area of about 150 × 150 μ m^2. The reflectance spectrum was normalized by the gold mirror.

Simulation. The simulated spectra were calculated by the numerical simulation software (COMSOL Multiphysics) based on the finite-element method (FEM). The refractive index of the fused silica substrate and SOG layer were set as 1.4584 and 1.41, respectively. The permittivity of gold was described by the Lorentz−Drude model with a damping constant of 0.07 eV and a plasma frequency of 8.997 eV. For the simulation of array structures, the periodic boundary condition was used along *x*- and *y*-directions. The incident wave was defined as either an *x*- or *y*-polarized plane wave. By calculating the scattering parameters (S-parameters), we could directly obtain the optical reflection as well as the transmission spectra.

ASSOCIATED CONTENT

Supporting Information

The Supporting Information is available free of charge on the ACS Publications website at DOI: 10.1021/acsnano.7b08828.

Electromagnetic multipole expansion; optical response of VSRR; optical spectra with electromagnetic multipole expansion; extinction spectra of the optical anapole metamaterial; optical response of toroidal metamaterials with *y*-polarized illumination; independence of electric and toroidal dipoles; and loss-dependence of anapole mode excitation (PDF)

Movie of the electromagnetic multipole evolution with different gap sizes (AVI)

AUTHOR INFORMATION

Corresponding Author

*E-mail: dptsai@sinica.edu.tw.

DOI: 10.1021/acsnano.7b08828
ACS Nano 2018, 12, 1920−1927

ORCID

Pin Chieh Wu: 0000-0002-5781-9696
Din Ping Tsai: 0000-0002-0883-9906

Notes

The authors declare no competing financial interest.

ACKNOWLEDGMENTS

The authors acknowledge financial support from the Ministry of Science and Technology, Taiwan (Grant No.: MOST-106-2745-M-002-003-ASP) and Academia Sinica (Grant No.: AS-103-TP-A06), the UK Engineering and Physical Sciences Research Council (Grant: EP/M009122/1), and the Singapore Ministry of Education (Grant: MOE2011-T3-1-005). They are also grateful to the National Center for Theoretical Sciences, NEMS Research Center of National Taiwan University, National Center for High-Performance Computing, Taiwan, and Research Center for Applied Sciences, Academia Sinica, Taiwan, for their supports. Following a period of embargo, the data from this article can be obtained from the University of Southampton research repository https://doi.org/10.5258/SOTON/D0136.

REFERENCES

(1) Esposito, S. Transition from Majorana to Weyl Fermions and Anapole Moments. *EPL (Europhysics Letters)* **2013**, *102*, 17006.
(2) Dubovik, V. M.; Martsenyuk, M. A.; Saha, B. Material Equations for Electromagnetism with Toroidal Polarizations. *Phys. Rev. E: Stat. Phys., Plasmas, Fluids, Relat. Interdiscip. Top.* **2000**, *61*, 7087−7097.
(3) Dubovik, V. M.; Tugushev, V. V. Toroid Moments in Electrodynamics and Solid-State Physics. *Phys. Rep.* **1990**, *187*, 145−202.
(4) Papasimakis, N.; Fedotov, V. A.; Savinov, V.; Raybould, T. A.; Zheludev, N. I. Electromagnetic Toroidal Excitations in Matter and Free Space. *Nat. Mater.* **2016**, *15*, 263−271.
(5) Tseng, M. L.; Yang, J.; Semmlinger, M.; Zhang, C.; Nordlander, P.; Halas, N. J. Two-Dimensional Active Tuning of an Aluminum Plasmonic Array for Full-Spectrum Response. *Nano Lett.* **2017**, *17*, 6034−6039.
(6) Wu, P. C.; Papasimakis, N.; Tsai, D. P. Self-Affine Graphene Metasurfaces for Tunable Broadband Absorption. *Phys. Rev. Appl.* **2016**, *6*, 044019.
(7) Zhang, R.; Bursi, L.; Cox, J. D.; Cui, Y.; Krauter, C. M.; Alabastri, A.; Manjavacas, A.; Calzolari, A.; Corni, S.; Molinari, E.; Carter, E. A.; García de Abajo, F. J.; Zhang, H.; Nordlander, P. How To Identify Plasmons from the Optical Response of Nanostructures. *ACS Nano* **2017**, *11*, 7321−7335.
(8) König, M.; Rahmani, M.; Zhang, L.; Lei, D. Y.; Roschuk, T. R.; Giannini, V.; Qiu, C.-W.; Hong, M.; Schlücker, S.; Maier, S. A. Unveiling the Correlation between Nanometer-Thick Molecular Monolayer Sensitivity and Near-Field Enhancement and Localization in Coupled Plasmonic Oligomers. *ACS Nano* **2014**, *8*, 9188−9198.
(9) Zhang, L.; Mei, S.; Huang, K.; Qiu, C.-W. Advances in Full Control of Electromagnetic Waves with Metasurfaces. *Adv. Opt. Mater.* **2016**, *4*, 818−833.
(10) Kabashin, A. V.; Evans, P.; Pastkovsky, S.; Hendren, W.; Wurtz, G. A.; Atkinson, R.; Pollard, R.; Podolskiy, V. A.; Zayats, A. V. Plasmonic Nanorod Metamaterials for Biosensing. *Nat. Mater.* **2009**, *8*, 867−871.
(11) Jahani, S.; Jacob, Z. All-Dielectric Metamaterials. *Nat. Nanotechnol.* **2016**, *11*, 23−36.
(12) Kaelberer, T.; Fedotov, V. A.; Papasimakis, N.; Tsai, D. P.; Zheludev, N. I. Toroidal Dipolar Response in a Metamaterial. *Science* **2010**, *330*, 1510−1512.
(13) Basharin, A. A.; Kafesaki, M.; Economou, E. N.; Soukoulis, C. M.; Fedotov, V. A.; Savinov, V.; Zheludev, N. I. Dielectric Metamaterials with Toroidal Dipolar Response. *Phys. Rev. X* **2015**, *5*, 011036.
(14) Liu, Z.; Du, S.; Cui, A.; Li, Z.; Fan, Y.; Chen, S.; Li, W.; Li, J.; Gu, C. High-Quality-Factor Mid-Infrared Toroidal Excitation in Folded 3D Metamaterials. *Adv. Mater.* **2017**, *29*, 1606298.
(15) Huang, Y.-W.; Chen, W. T.; Wu, P. C.; Fedotov, V.; Savinov, V.; Ho, Y. Z.; Chau, Y.-F.; Zheludev, N. I.; Tsai, D. P. Design of Plasmonic Toroidal Metamaterials at Optical Frequencies. *Opt. Express* **2012**, *20*, 1760−1768.
(16) Ögüt, B.; Talebi, N.; Vogelgesang, R.; Sigle, W.; van Aken, P. A. Toroidal Plasmonic Eigenmodes in Oligomer Nanocavities for the Visible. *Nano Lett.* **2012**, *12*, 5239−5244.
(17) Gupta, M.; Savinov, V.; Xu, N.; Cong, L.; Dayal, G.; Wang, S.; Zhang, W.; Zheludev, N. I.; Singh, R. Sharp Toroidal Resonances in Planar Terahertz Metasurfaces. *Adv. Mater.* **2016**, *28*, 8206−8211.
(18) Wei, L.; Xi, Z.; Bhattacharya, N.; Urbach, H. P. Excitation of the Radiationless Anapole Mode. *Optica* **2016**, *3*, 799−802.
(19) Miroshnichenko, A. E.; Evlyukhin, A. B.; Yu, Y. F.; Bakker, R. M.; Chipouline, A.; Kuznetsov, A. I.; Luk'yanchuk, B.; Chichkov, B. N.; Kivshar, Y. S. Nonradiating Anapole Modes in Dielectric Nanoparticles. *Nat. Commun.* **2015**, *6*, 8069.
(20) Nemkov, N. A.; Basharin, A. A.; Fedotov, V. A. Nonradiating Sources, Dynamic Anapole, and Aharonov-Bohm Effect. *Phys. Rev. B: Condens. Matter Mater. Phys.* **2017**, *95*, 165134.
(21) Fedotov, V. A.; Rogacheva, A. V.; Savinov, V.; Tsai, D. P.; Zheludev, N. I. Resonant Transparency and Non-Trivial Non-Radiating Excitations in Toroidal Metamaterials. *Sci. Rep.* **2013**, *3*, 2967.
(22) Li, J.; Zhang, Y.; Jin, R.; Wang, Q.; Chen, Q.; Dong, Z. Excitation of Plasmon Toroidal Mode at Optical Frequencies by Angle-Resolved Reflection. *Opt. Lett.* **2014**, *39*, 6683−6686.
(23) Dong, Z.-G.; Zhu, J.; Yin, X.; Li, J.; Lu, C.; Zhang, X. All-optical Hall Effect by the Dynamic Toroidal Moment in a Cavity-based Metamaterial. *Phys. Rev. B: Condens. Matter Mater. Phys.* **2013**, *87*, 245429.
(24) Dong, Z.-G.; Zhu, J.; Rho, J.; Li, J.-Q.; Lu, C.; Yin, X.; Zhang, X. Optical Toroidal Dipolar Response by an Asymmetric Double-Bar Metamaterial. *Appl. Phys. Lett.* **2012**, *101*, 144105−144105−4.
(25) Savinov, V.; Fedotov, V. A.; Zheludev, N. I. Toroidal Dipolar Excitation and Macroscopic Electromagnetic Properties of Metamaterials. *Phys. Rev. B: Condens. Matter Mater. Phys.* **2014**, *89*, 205112.
(26) Radescu, E. E.; Vaman, G. Exact Calculation of the Angular Momentum Loss, Recoil Force, and Radiation Intensity for an Arbitrary Source in terms of Electric, Magnetic, and Toroid Multipoles. *Phys. Rev. E: Stat. Phys., Plasmas, Fluids, Relat. Interdiscip. Top.* **2002**, *65*, 046609.
(27) Wu, P. C.; Chen, W. T.; Yang, K.-Y.; Hsiao, C. T.; Sun, G.; Liu, A. Q.; Zheludev, N. I.; Tsai, D. P. Magnetic Plasmon Induced Transparency in Three-Dimensional Metamolecules. *Nanophotonics* **2012**, *1*, 131−138.
(28) Wu, P. C.; Sun, G.; Chen, W. T.; Yang, K.-Y.; Huang, Y.-W.; Chen, Y.-H.; Huang, H. L.; Hsu, W.-L.; Chiang, H. P.; Tsai, D. P. Vertical Split-Ring Resonator based Nanoplasmonic Sensor. *Appl. Phys. Lett.* **2014**, *105*, 033105.
(29) Wu, P. C.; Liao, C. Y.; Chen, J.-W.; Tsai, D. P. Isotropic Absorption and Sensor of Vertical Split-Ring Resonator. *Adv. Opt. Mater.* **2017**, *5*, 1600581.
(30) Wu, P. C.; Hsu, W.-L.; Chen, W. T.; Huang, Y.-W.; Liao, C. Y.; Liu, A. Q.; Zheludev, N. I.; Sun, G.; Tsai, D. P. Plasmon Coupling in Vertical Split-Ring Resonator Metamolecules. *Sci. Rep.* **2015**, *5*, 9726.
(31) Fan, K.; Strikwerda, A. C.; Zhang, X.; Averitt, R. D. Three-Dimensional Broadband Tunable Terahertz Metamaterials. *Phys. Rev. B: Condens. Matter Mater. Phys.* **2013**, *87*, 161104.
(32) Liu, W.; Zhang, J.; Lei, B.; Hu, H.; Miroshnichenko, A. E. Invisible Nanowires with Interfering Electric and Toroidal Dipoles. *Opt. Lett.* **2015**, *40*, 2293−2296.
(33) Guo, L.; Li, M.; Ye, Q.; Xiao, B.; Yang, H. Electric Toroidal Dipole Response in Split-Ring Resonator Metamaterials. *Eur. Phys. J. B* **2012**, *85*, 1−5.
(34) Fan, Y.; Wei, Z.; Li, H.; Chen, H.; Soukoulis, C. M. Low-Loss and High-Q Planar Metamaterial with Toroidal Moment. *Phys. Rev. B: Condens. Matter Mater. Phys.* **2013**, *87*, 115417.

DOI: 10.1021/acsnano.7b08828
ACS Nano 2018, 12, 1920−1927

(35) Grinblat, G.; Li, Y.; Nielsen, M. P.; Oulton, R. F.; Maier, S. A. Efficient Third Harmonic Generation and Nonlinear Subwavelength Imaging at a Higher-Order Anapole Mode in a Single Germanium Nanodisk. *ACS Nano* **2017**, *11*, 953−960.
(36) Grinblat, G.; Li, Y.; Nielsen, M. P.; Oulton, R. F.; Maier, S. A. Enhanced Third Harmonic Generation in Single Germanium Nanodisks Excited at the Anapole Mode. *Nano Lett.* **2016**, *16*, 4635−4640.
(37) Wang, R.; Dal Negro, L. Engineering Non-radiative Anapole Modes for Broadband Absorption Enhancement of Light. *Opt. Express* **2016**, *24*, 19048−19062.
(38) Huang, Y.-W.; Chen, W. T.; Wu, P. C.; Fedotov, V. A.; Zheludev, N. I.; Tsai, D. P. Toroidal Lasing Spaser. *Sci. Rep.* **2013**, *3*, 1237.
(39) Totero Gongora, J. S.; Miroshnichenko, A. E.; Kivshar, Y. S.; Fratalocchi, A. Anapole Nanolasers for Mode-Locking and Ultrafast Pulse Generation. *Nat. Commun.* **2017**, *8*, 15535.

DOI: 10.1021/acsnano.7b08828
ACS Nano 2018, 12, 1920−1927